MAP-0/824
For Author's Correction Only

Meteorol Atmos Phys 000, 1–14 (2006)
DOI 10.1007/s00703-006-0229-0
Printed in The Netherlands

Meteorology and Atmospheric Physics

International Pacific Research Center, Department of Meteorology, University of Hawaii, Honolulu, Hawaii, USA

Simulation of formation of a near-equatorial typhoon Vamei (2001)

C. R. S. Chambers and **T. Li**

With 12 Figures

Received June 28, 2006; accepted November 1, 2006
Published online: • •, 2006

Summary

A community mesoscale model is used to simulate and understand processes that led to the formation and intensification of the near-equatorial typhoon Vamei that formed in the South China Sea in December, 2001. The simulated typhoon resembles the observed in that it had a short lifetime and a small size, formed near the equator (south of 2° N), and reached category-one intensity. The formation involved the interactions between the scales of the background cyclonic circulation (the Borneo Vortex of order ∼100 km) and of mesoscale convective vortices (MCVs, in the order ∼10 km). Before tropical cyclone formation MCVs formed along a convergent, horizontal shear vorticity line on the eastern edge of an exceptionally strong monsoonal northerly wind surge.

The typhoon genesis is marked by three rapid intensification periods, which are associated with the rapid growth of potential vorticity (PV). A vorticity budget analysis reveals that the increases in low-level vorticity during the rapid intensification periods are attributed to enhanced horizontal vorticity fluxes into the storm core. The increase of the horizontal vorticity flux is associated with the merging of areas of high PV associated with MCVs into the storm core as they are advected by background cyclonic flows. The increases in PV at upper levels are associated with the evaporation of upper level stratiform precipitation and increases of vertical potential temperature gradient below the maximum stratiform cloud layer. It appears that two key sources of PV at upper and lower levels are crucial for the build up of high PV and a deepening of a cyclonic layer throughout the troposphere.

1. Introduction

On the 27 December 2001, the tropical cyclone (TC) Vamei formed at 1.5° N north of the equator in the South China Sea (SCS). This typhoon is the most near-equatorial TC reported by the Joint Typhoon Warning Center (JTWC, 2002), confirmed by the measurement of sustained winds of 75 knots on a US naval ship. The ship's radar indicated a distinct eye in Vamei, consistent with TRMM images (Padgett, 2001). Vamei kept its typhoon strength for about 12 hours, and then weakened rapidly after making landfall in Malaysia.

The formation of Typhoon Vamei was first discussed by Chang et al (2003) from an observational perspective. They noted that the formation was associated with an exceptionally strong and persistent northerly cold surge that turned anticlockwise near the equator. This caused a large-scale cyclonic vorticity in the southern SCS. Meanwhile, the Borneo Vortex, a quasi-stationary low pressure system that frequently forms on the lee (west) side of Borneo, drifted westward and towards the equatorial region. It is the complex interaction between the mesoscale vortex and large-scale background cyclonic flow that led to the typhoon formation. By calculating the probability of the exceptional strength and longevity of the cold surge and frequency of the Borneo Vortex, they concluded that such a low-latitude TC genesis may only occur once every century.

Historically, no typhoons had been recorded within 3 degrees of the equator. It was thought impossible due to the negligible Coriolis force at such low latitudes. Anthes (1982) argued that in order to effectively generate a rotational motion a TC must form beyond 6° latitude. This argument is consistent with the vast majority of observed TC tracks. There have however been notable exceptions. One example is typhoon Sarah (1967), which reached typhoon strength at 3.3° N, 146.8° E. Another is typhoon Kate (1970) that was observed at 5° N for 72 hours (Holliday and Thompson, 1986). Described as a "microstorm", Kate had an eye diameter of 31 km on 16 October. Deep convection was confined to the eyewall with minor rainband activity outside of the eyewall. The small eye and weak rainbands of typhoon Vamei (Padgett, 2001) exhibited characteristics similar to Kate.

Typhoons that form within 10° latitude of the equator often exhibit the characteristics of a small size and rapid intensification. Numerical experiments by DeMaria and Pickle (1988) suggested that the size of a TC became smaller when it was positioned in lower latitudes. This is because a smaller Coriolis force leads to the penetration of low-level moisture into the TC core region. This concentrates diabatic heating near the TC center in the wall of a small eye. They speculated that the lack of TCs close to the equator in the real atmosphere is attributed to the difficulty in maintaining a convectively driven vortex in the presence of vertical shear when the scale of the vortex is too small. In fact, typhoon Vamei rapidly intensified, developed a small eye, and remained at typhoon strength for only a short period of time.

Various theories have been proposed to understand TC genesis. They include the conditional instability of the second kind (CISK, Charney and Eliasen, 1964) and wind-induced surface heat exchange (WISHE, Rotunno and Emanuel, 1987). Montgomery and Enagonio (1998) suggested that the intensification of a weak vortex could proceed through the axisymmetrization of convectively forced low-level potential vorticity (PV) anomalies. Building on this idea, Hendricks et al (2004) stated that the increase in the vertical gradient of diabatic heating in the low troposphere ($z < 5$ km) associated with vortical "hot towers" led to an increase in lower tropospheric PV below the diabatic heating maximum. Bister and Emanuel (1997) proposed that the evaporation of mesoscale precipitation below an upper level stratiform cloud deck associated with a pre-existing mesoscale convective system (MCS) might create an elevated vertical diabatic heating gradient below the stratiform cloud base. Consequently the vertical gradient in potential temperature increases, which in turn increases local PV, contributing to the formation of a cold core mid-level mesocyclone. Mesoscale subsidence could further enable the vortex to propagate downward. The consequent deep vortex might provide the ideal embryo for tropical cyclogenesis through the eruption of new convection and the development of a warm core vortex.

Can one use the theories above to explain the near-equatorial TC genesis? The aim of this study is twofold. First we intend to simulate this TC genesis event using a mesoscale model. Secondly, we intend to investigate specific processes that give rise to the cyclogenesis. The focus of this study is on the formation and intensification period of the simulation, with a detailed analysis of vorticity budget in a storm-following grid. The organization of this paper is as follows. In Sect. 2, the setup of the simulation is described. Section 3 describes the evolution of the simulation. Section 4 discusses the roles of the generation and merging of mesoscale convective vortices and the upper level stratiform rain mechanism on the intensification. Section 5 examines the terms in the vorticity equation near the level of maximum vorticity during intensification. Section 6 summarizes our results and presents out conclusions.

2. Model and experiment design

The model to be used for the simulation is the fifth-generation National Centers for Atmospheric Research (NCAR)/Penn State mesoscale model (MM5) (see Dudhia, 1993, for model details). Two domains, an outer and inner one shown in Fig. 1, were used with horizontal resolutions of 27 and 9 km, respectively. The physics schemes used in this simulation were similar to those used by Braun and Tao (2000), which included the

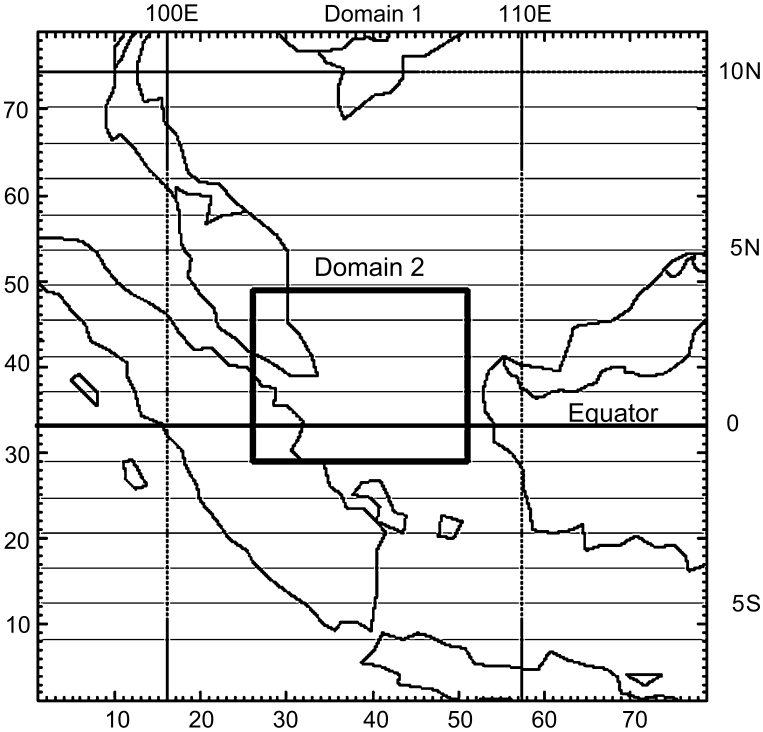

Fig. 1. Map showing the area covered by domain 1 (27 km resolution, entire map with grid points shown along the left and bottom sides) and domain 2 (9 km resolution, thick lined rectangle). Horizontal lines are for every degree of latitude

Burk-Thompson PBL (Burk and Thompson, 1989) scheme, the Betts–Miller cumulus scheme, and the simple ice explicit moisture scheme of Dudhia (1989).

No bogus initialization scheme is used. The model was run for 96 hours, starting from 0000 UTC 24 December, 3 days prior to the TC formation. This corresponds to a local time for Malaysia 0800 LT 24 December. The model was initialized using the NCEP Global Tropospheric Analyses (http://dss.ucar.edu/datasets/ds083.2). This dataset is available at 6-hourly intervals, has 24 levels in the vertical, and a horizontal resolution of $1^\circ \times 1^\circ$ (latitude, longitude).

3. Simulation results

During the first 20 hours of the simulation, the atmospheric conditions in the SCS became more favorable for TC genesis because of the presence of an unusually strong and persistent surge of northerly winds. Figure 2a shows that at hour 19, strong surface northerly winds from the surge protrude through the central and eastern SCS all the way to the equator. Near the equator can be seen a cyclonic circulation developed over the eastern SCS as this surge turned westward south of the equator and then northward in the east SCS. The model simulates a distinct convergent horizontal shearline with embedded smaller scale low pressure centers (Fig. 2b). These smaller mesoscale convective vortices (MCVs) developed along the strong convergence line on the eastern flank of the northerly surge (Fig. 2c). The strong convergence concentrates moisture in the region, producing a high relative humidity band. This helped fuel the convection that generated the MCVs. The role of the MCVs in the TC vorticity buildup will be discussed in the next section. The strong northerly winds over relatively warm (26–27 °C) SST produced large latent heat fluxes (200–350 W m^{-2}) throughout the northerly surge region at the surface (Fig. 2d). Thus both the surface evaporation and the convergence favor a buildup of boundary layer moisture along the shearline that, through advection of the background mean flow, transports the moisture equatorward and toward the cyclogenesis region.

Upper level winds were in general weak and divergent during the initial stage. The intense convection at hour 19 over the low-level convergence line enhanced the upper level divergence, leading to $\sim$20 m s^{-1} outflow at 200 mb that spread westward from the line (not shown). This enabled a favorable outflow channel to the west

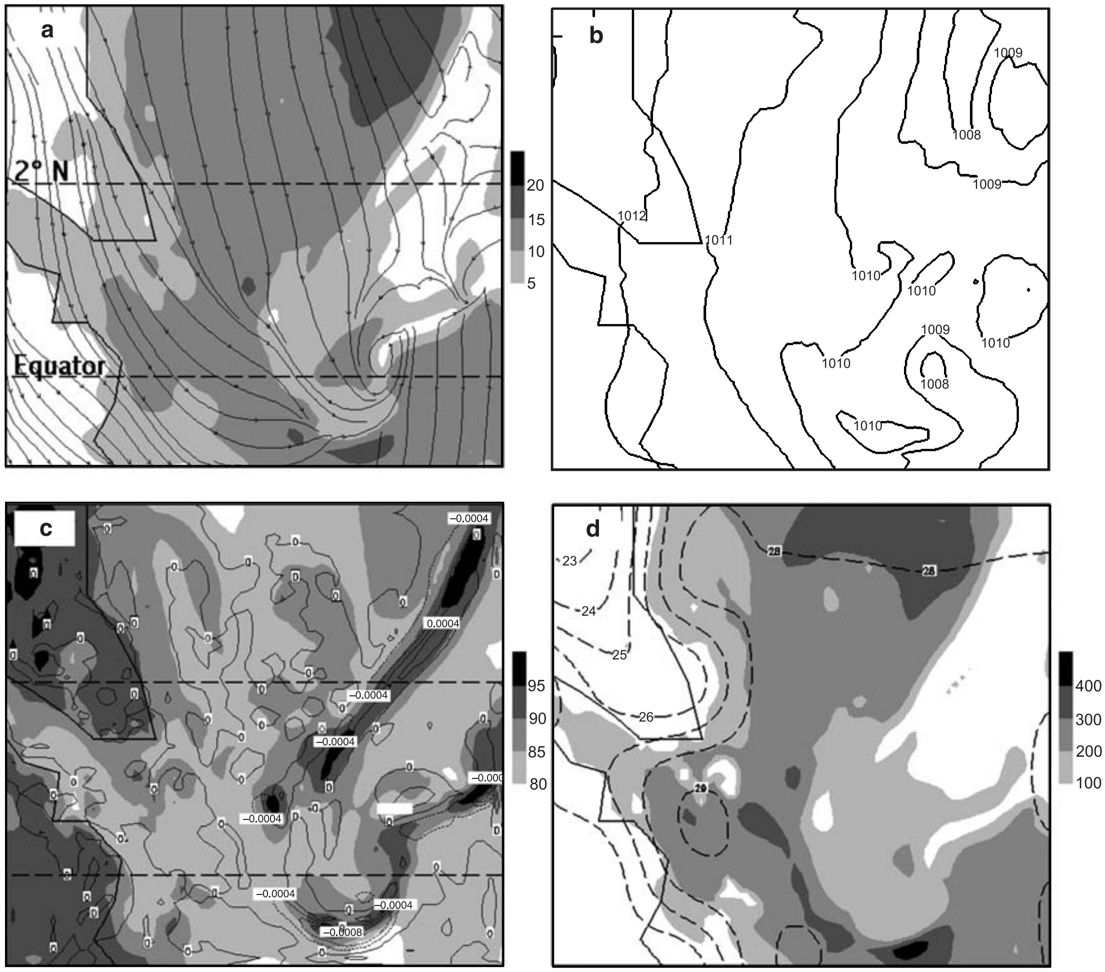

Fig. 2. Domain 2 (**a**) surface isotachs m s^{-1} and streamlines, (**b**) sea-level pressure (mb) for hour 19 of the simulation (1800 UTC 24 December, 2001), (**c**) divergence (thin contours in s^{-1}) and relative humidity (shaded contours in %), and (**d**) sea-surface temperature (thick dashed contours in °C) and latent heat flux (shaded contours in W m^{-2})

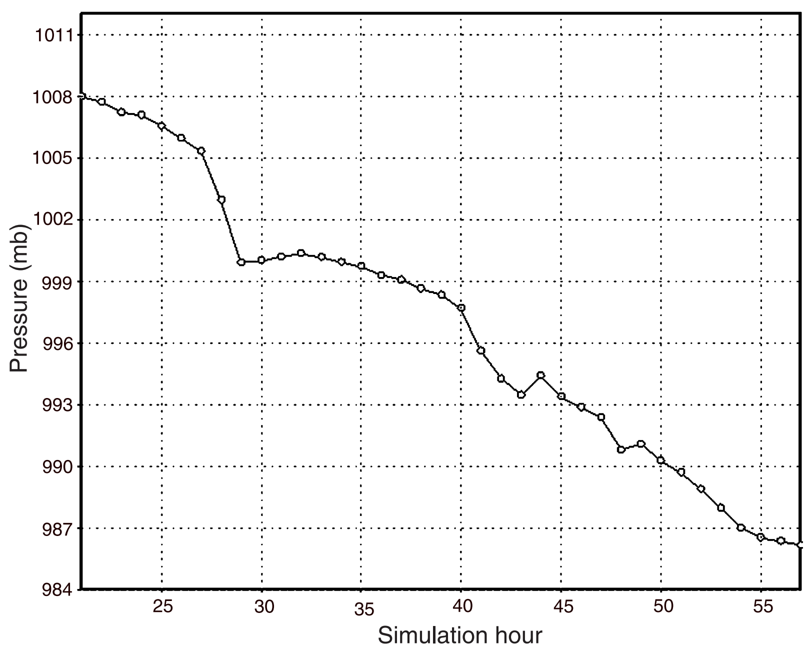

Fig. 3. Central surface pressure for hours 21–57

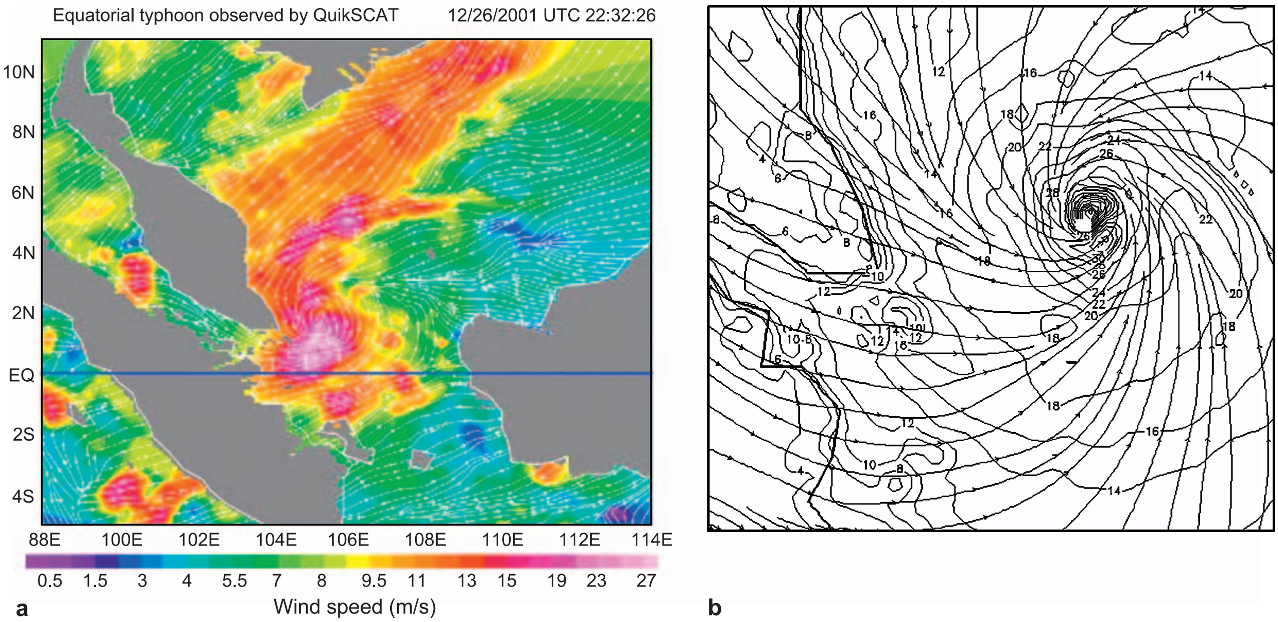

Fig. 4a. Observed Quickscat wind speeds (colors) and streamlines at 22:32 UTC on the 26 Dec. (from Chang et al, 2003). (**b**) Modelled surface isotachs ($\mathrm{m\,s^{-1}}$) and streamlines for the time of maximum surface wind speed (hour 59 of the simulation). Maximum wind speeds were $36\,\mathrm{m\,s^{-1}}$

of Borneo, and helped to maintain vigorous convection along the shearline.

Figure 3 shows time evolution of the storm's central minimum surface pressure. It dropped 22 mb in the 36 hours from hours 21–57 (i.e., 24/2100 UTC to 26/0900 UTC). This period will be referred to as the "intensification period". At hour 21, a closed low-pressure system was observed at the first time, with maximum winds greater than $17\,\mathrm{m\,s^{-1}}$ (a tropical depression intensity as defined by the National Hurricane Center, Landsea, 2006). By the end of this intensification period (at hour 57), the storm achieved its lowest central pressure of 986 mb. The pressure curve is punctuated with two obvious periods of rapid intensification (RI) during hours 27–29 and hours 40–44. These periods are hereafter referred to as RI1 and RI2, respectively. A lesser pressure drop occurs at hour 47 and is defined as RI3.

The model TC reached Typhoon strength ($33\,\mathrm{m\,s^{-1}}$, 64 kt) at hour 46 at 1.5° N. After that, the storm weakened a little bit, and then re-attained typhoon strength at hour 56 at 1.7° N and remained so for 7 hours. The model simulated maximum surface winds of $37\,\mathrm{m\,s^{-1}}$ (72 kt) during the peak phase of the TC, as shown in Fig. 4b. A comparison with the Quickscat winds (Fig. 4a) shows that the modeled tropical cyclone has a similar size and intensity. The diameter of the eye, as estimated based on the model surface wind profile, is 30–45 km, with an oval shape of the eye. This size compares well to Padgett's (2001) estimates from TRMM and SSMI imagery (~39 km at 27/0030 UTC and ~28 km at 27/0220 UTC, respectively). The major deficiency of the model simulation is that the modeled TC reached its maximum intensity 12 hours earlier than the actual storm. The location of the simulated TC was shifted slightly to the east and consequently it had more time to propagate northwestward before landfall. The significant result, however, is that the model successfully generated a small short-lived typhoon that first reached typhoon strength at 1.7° N.

4. Formation mechanisms

In this section, we examine possible mechanisms responsible for the Vamei formation. In particular, the potential vorticity (PV) field will be analyzed during the formation and intensification period. Our aim is to look for evidence for the generation and merging of low

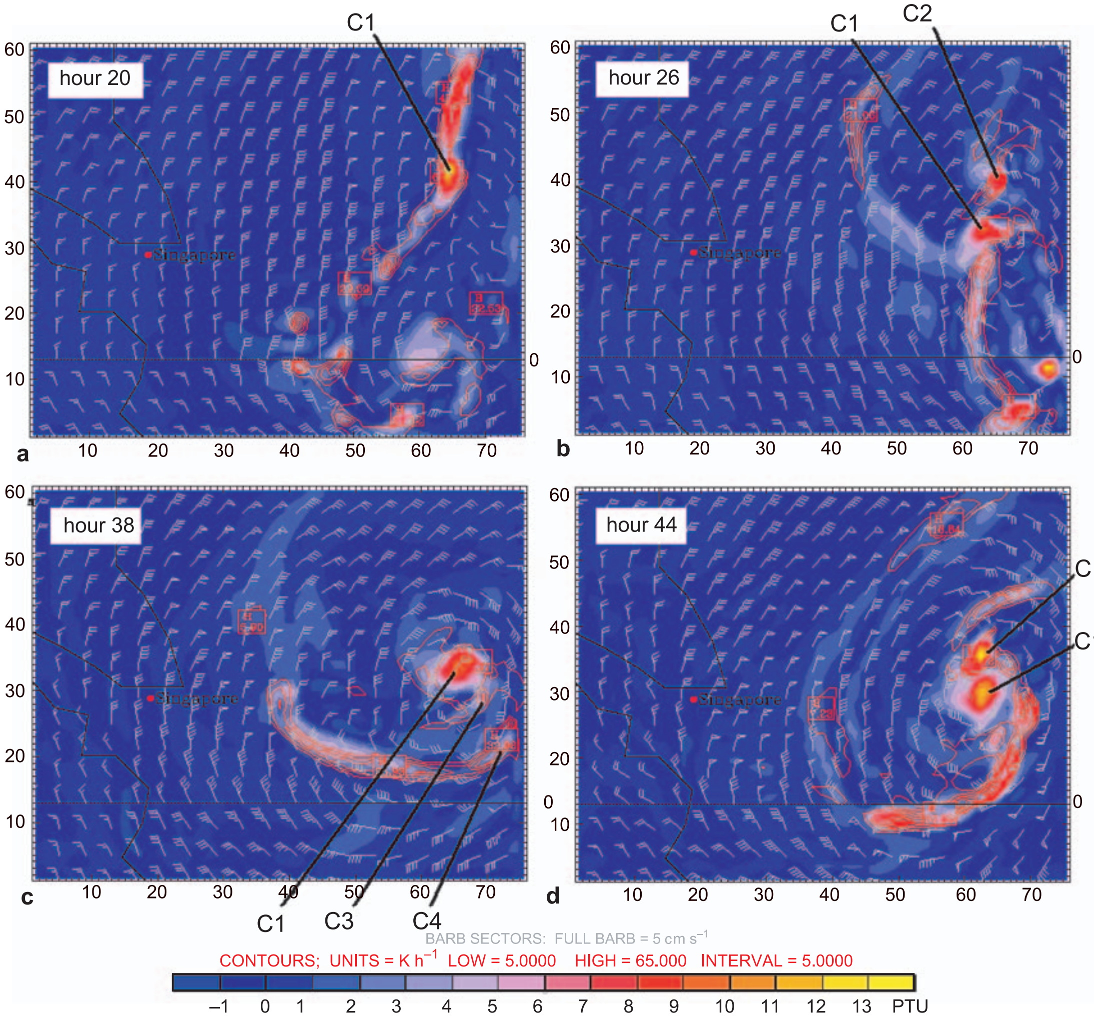

Fig. 5. Potential vorticity (PVU as color shaded contours), condensational heating (red contours in K h^{-1}) and winds(barbs) at $\sigma = 0.788$ for (**a**) hour 20, (**b**) hour 26, (**c**) hour 38, and (**d**) hour 44 of the simulation. The locations of the notable MCVs are labeled where C1 is the dominant MCV that becomes the storm center

tropospheric PV in the MCVs and the effect of the stratiform rain in the upper tropospheric PV generation.

4.1 Formation and merging of mesoscale convective vortices (MCVs)

Analysis of the PV field at $\sigma = 0.788$ (Fig. 5) for hours 25–55 shows features that correlate well with the hot tower hypothesis. The generation of PV in MCVs requires background vorticity. Before formation this vorticity is provided by the eastern edge of the surge of northerly winds encountering light winds to the east (Fig. 2a). The resulting horizontal shear vorticity lies in a convergent flow region, triggering numerous areas of deep convection.

This high PV is related to the high relative vorticity combined with the large vertical gradient in diabatic heating below the diabatic heating maximum. Figure 5 shows that areas of high PV are frequently co-located with areas of diabatic heating. On the large scale the SCS has cyclonic flows that advect the mesoscale PV anomalies first southward then eastward and northward. In this manner the large-scale flow aids in the concentration of convectively generated low-level PV anomalies within the cyclonic circulation to the west of Borneo.

The TC genesis may be well traced back to the development and evolution of MCVs. At hour 20, a strong MCV (denoted as C1 in Fig. 5a). Advected by the large-scale cyclonic flow, this MCV co-located with the cyclonic circulation

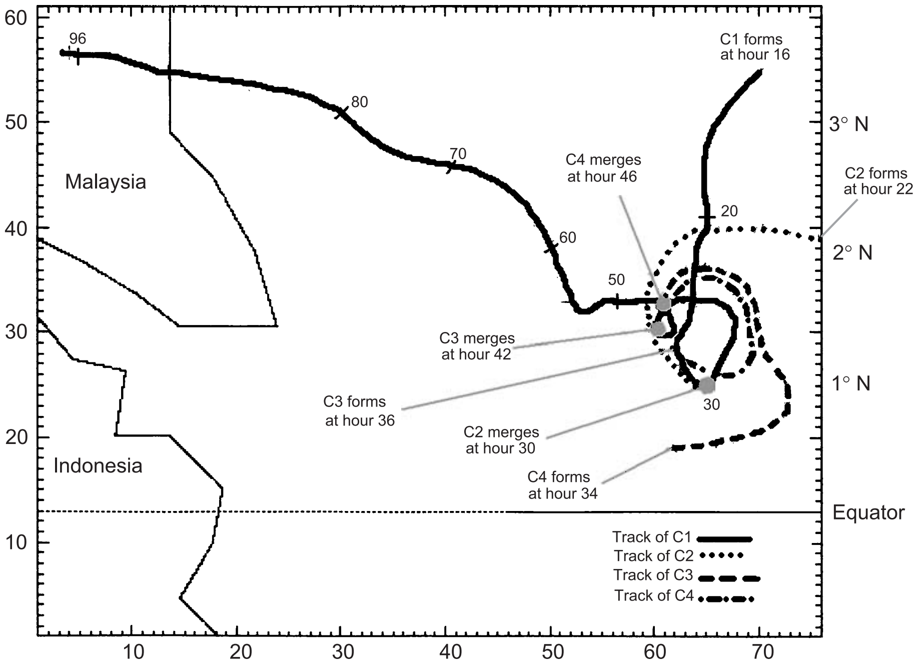

Fig. 6. Track of the MCV that later becomes the storm center (C1) as well as the tracks of the MCVs that merged with C1 during the RI periods

center at hour 26. Meanwhile another strong MCV (denoted as C2 in Fig. 5b) appeared to the north of C1.

From this time on, the intensification of the tropical cyclone proceeds as C1 absorbs positive PV anomalies from either existing or former convective areas. The axisymmetrization of the PV anomalies occurs as the numerous MCVs merge into the large-scale vorticity center, leading to a buildup of high PV in C1 (Fig. 5c and d). As the convergence line wraps around the south of the circulation center, it takes the form of a dominant rainband of the TC and provides a stream of convectively generated PV anomalies that feed into the developing storm core.

The rapid intensification periods (RI1 and RI2) occur when particularly dramatic mergers occur as convective anomalies (C2 and C3, respectively) that spiral into the core as shown in Fig. 6. The evolution of the RI1 and RI2 periods are represented in Fig. 7. It is evident by looking at the integrated cloud water for both periods, that the drop in surface pressure occurred as a deep convective region merged with the eyewall. For both periods the associated convection wrapped around to the northwestern side of the storm center as the rate of decrease in central pressure reached its maximum. The northwest side of the storm lies in the track of the storm, and for both periods the storm exhibited a slowing of forward propagation as it digested the sibling convective region.

Further insight into the RI periods can be gained by looking at storm-centered, area-averaged plots. Figure 8a shows that both RI1 and RI2 occur during times of enhanced low-level convergence and vertical motion. This is a signal of enhanced convection associated with the merging of MCVs. Enhanced vertical motion should tend to increase the vorticity of the storm core through the stretching of the vortical column of air. The area-averaged vorticity in Fig. 8b shows a maximum in the low levels ($\sigma = 0.95$–0.9). The most rapid vorticity increases are associated with the rapid intensification periods and upward vorticity transport throughout the troposphere as the intensification proceeds.

Evidence for hot tower processes can be gained from Figs. 8c, b, and 9. During RI1 and RI2 we observe a downward development of larger vertical gradients in potential temperature from $\sigma = 0.7$ to 0.9. This downward development, on one hand, leads to a transition from unstable to stable stratification in the lower troposphere, and on the other hand helps increase local PV. Both the enhanced vorticity and vertical gradient in potential temperature contribute to elevated PV at $\sigma \sim 0.9$ (Fig. 9). This suggests that during the merger process strong diabatic heating in intense convection is acting to increase the

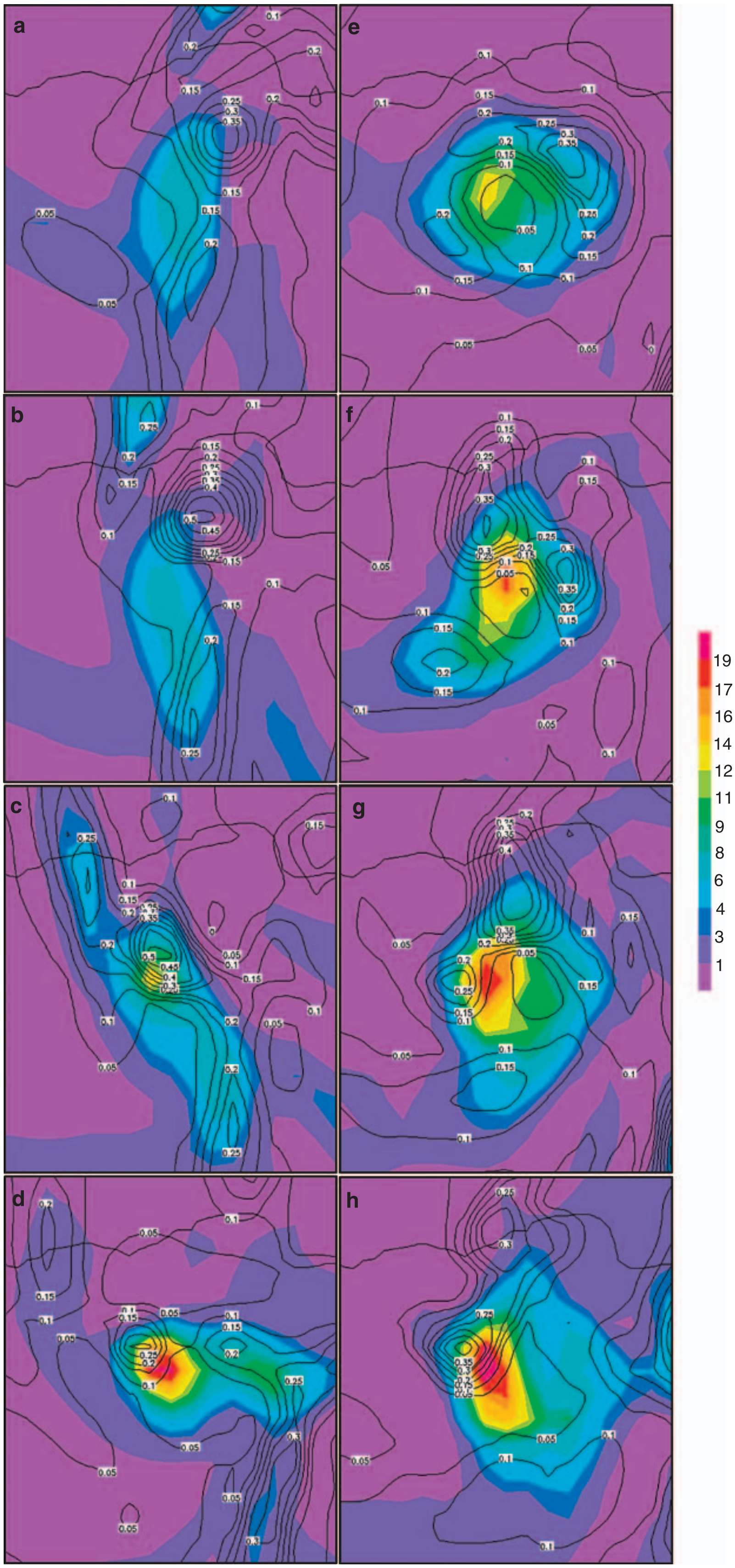

Fig. 7. 13 by 13 grid point boxes (117 km by 117 km) centered on the point of minimum pressure showing potential vorticity (PVU in colors) and integrated cloud water (black contours in cm) for the first and second rapid intensification periods RI1 (a–d) and RI2 (e–h)

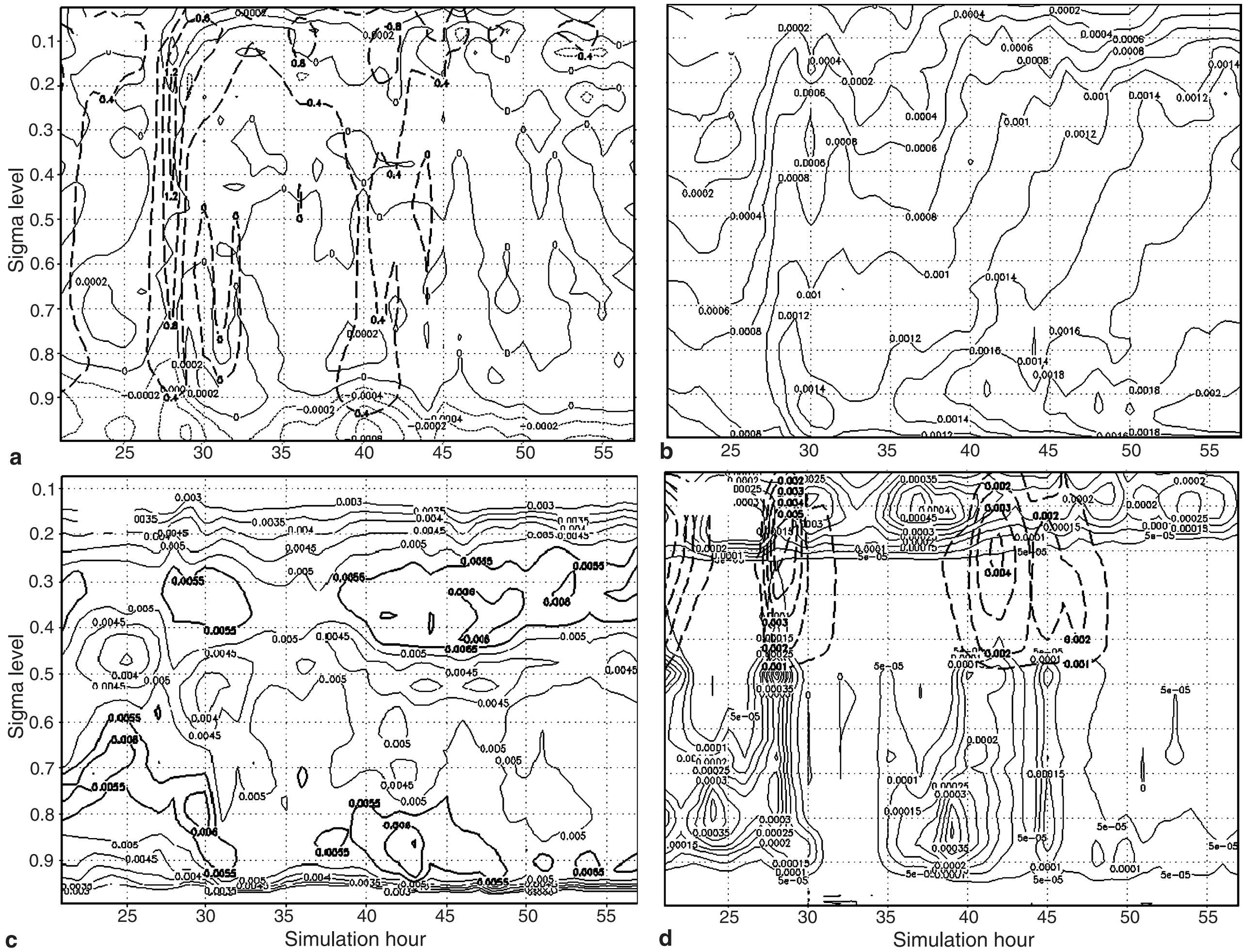

Fig. 8. Area averaged plots of (**a**) divergence (s^{-1}) and vertical velocity (dashed contours in m s^{-1}), (**b**) vorticity (s^{-1}), (**c**) vertical potential temperature gradient (K m^{-1}), and (**d**) cloud water (kg kg^{-1}) and rain water (bold dashed kg kg^{-1}) for a 6 by 6 grid point box (51 km × 51 km) centered on the storm center for the intensification period (hours 20–57)

PV below the heating maximum, which is consistent with the hot tower theory (e.g., Hendricks et al, 2004).

4.2 PV generation below the upper-level stratiform anvil clouds

In addition to a vertical potential temperature gradient maximum at low level, there is also a maximum at upper level ($\sigma = 0.35$) below the cloud water maximum (Fig. 8c and d). This increase in the vertical potential temperature gradient is caused by the contrast between latent heating within the stratiform clouds and evaporative cooling of stratiform precipitation below. This enhanced temperature gradient leads to the increase of PV at upper levels (Fig. 9).

The rain-water maxima occur during the three RI periods. Below the rain-water maxima the decrease in rain-water content is attributed to evaporation of rain drops. A correlation between the vertical potential temperature gradient maxima and maximum rain-water evaporation can be seen from Fig. 8c and d. At the beginning of the period (hour 20), there are a maximum in the rain water and an associated maximum in the vertical potential temperature gradient. Yet there is low PV at this time (Fig. 9). This is because the relative vorticity is low at the beginning of the period at upper levels (Fig. 8b). Overall, the simulation results suggest that the stratiform rainfall plays

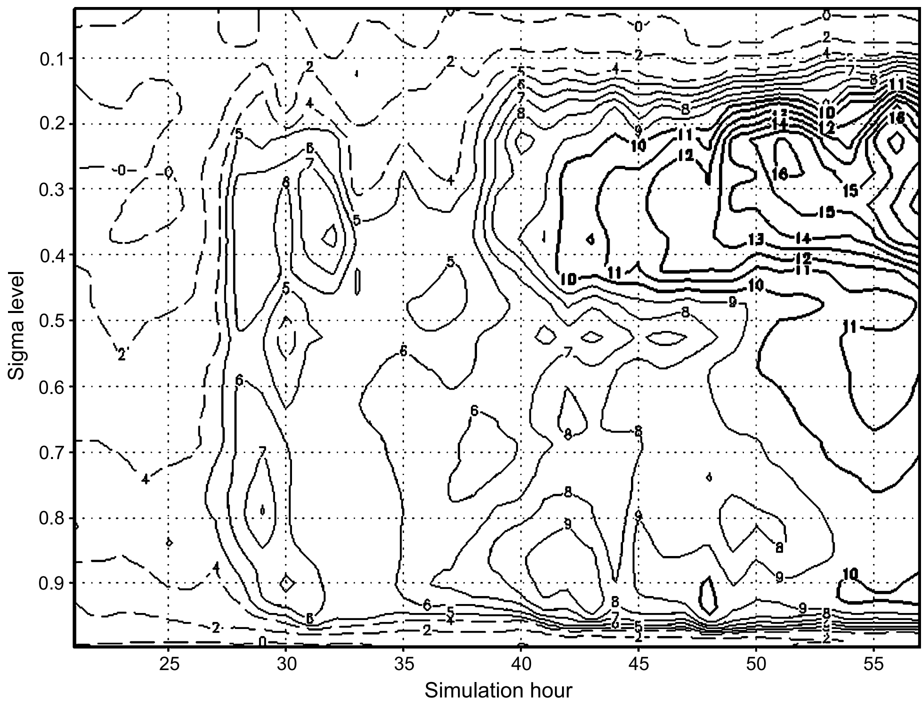

Fig. 9. As Fig. 11 for potential vorticity (PVU) where dashed contours are for PVU less than 5 and bold contours are for PVU greater than 9

an important role in building up the upper-level PV, serving as an additional factor to contribute to the rapid intensification of the TC.

5. Vorticity budget analysis

The purpose of this analysis is to examine which terms are most important in the vorticity growth near the core of the storm. Here we focus on the levels above and below the level of maximum vorticity that lies between $\sigma = 0.95$ and 0.90 (see Fig. 8b). The vorticity tendency terms are area-averaged over a 6×6 grid point box ($54\,\mathrm{km} \times 54\,\mathrm{km}$) centered on the minimum pressure (consistent with the analyses in previous sections). The vorticity equation (ignoring the solenoidal term)

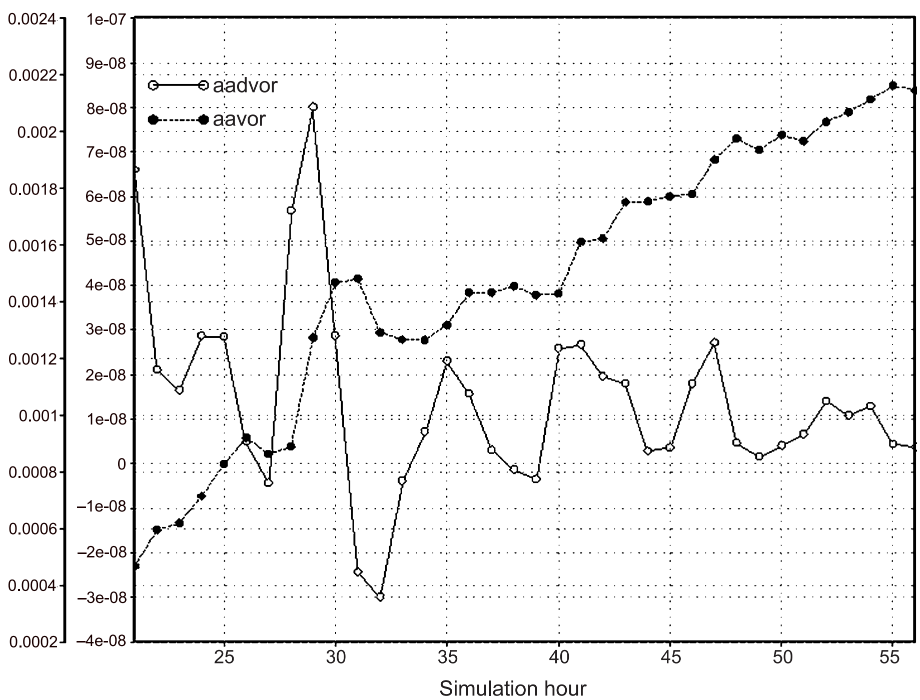

Fig. 10. Vorticity (s^{-1}) at sigma level = 0.95 (filled dots with left y-axis as scale) and vorticity change (s^{-2}), area averaged over a 54 km by 54 km storm centered box. Time on the x-axis covers the intensification period

may be written as (see Holton, 1992)

$$\frac{\partial \zeta}{\partial t} = \underbrace{-u\frac{\partial \zeta}{\partial x} - v\frac{\partial \zeta}{\partial y}}_{v_{\mathrm{adv}}} \underbrace{- w\frac{\partial \zeta}{\partial z}}_{vw_{\mathrm{adv}}} \underbrace{- \zeta\left(\frac{\partial u}{\partial x} + \frac{\partial v}{\partial y}\right)}_{v_{\mathrm{div}}} \underbrace{- \left(\frac{\partial w}{\partial x}\frac{\partial v}{\partial z} - \frac{\partial w}{\partial y}\frac{\partial u}{\partial z}\right)}_{v_{\mathrm{tilt}}}, \qquad (1)$$

where u, v, and w are zonal, meridional, and vertical velocity, respectively and ζ is the absolute vorticity. The first two terms on the right-hand side of Eq (1) are horizontal vorticity advection denoted as v_{adv}, the third term vertical vorticity advection denoted as vw_{adv}, the fourth and fifth terms are horizontal vorticity divergence denoted as v_{div}, and the last two terms are tilting/twisting represented by v_{tilt}. The planetary vorticity divergence term is about two orders of magnitude less than that of the relative vorticity divergence term due to the strong background vorticity in the region. This implies that the convergence of planetary vorticity plays a minor role in the vorticity development.

The increase in area-averaged vorticity at $\sigma = 0.95$ over the intensification period can be seen in Fig. 10. The largest rate of vorticity increase occurs at hour 29. This is related to the merging of C2 with C1 (RI1). A peak in vorticity change at hour 42 is associated with RI2 and a peak at hour 47 is associated with RI3. Similar vorticity increases also occur at hours 24 and 35 when a minor merger occurred, which led to enhanced hot tower activity near the core of the storm and thus a rise in vorticity. It is concluded that the merg-

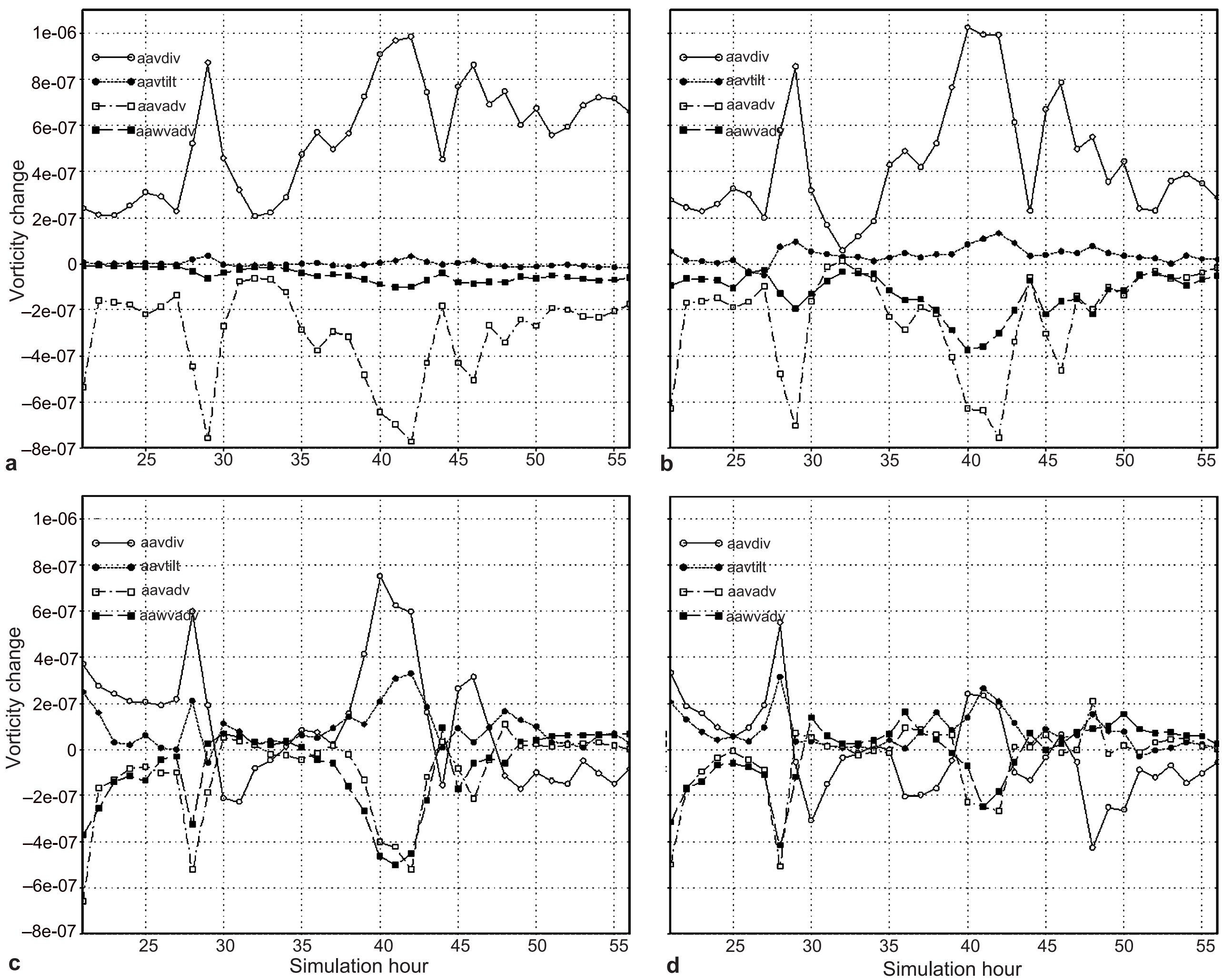

Fig. 11. The terms of the vorticity equation for a 6 by 6 grid point box centered on the point of minimum pressure. The boxes shown are for (**a**) $\sigma = 0.99$, (**b**) $\sigma = 0.95$, (**c**) $\sigma = 0.90$, and (**d**) $\sigma = 0.85$ where aavdiv is vorticity divergence, aavtilt is vorticity tilting, aavadv is horizontal vorticity advection, and aawvadv is vertical vorticity advection

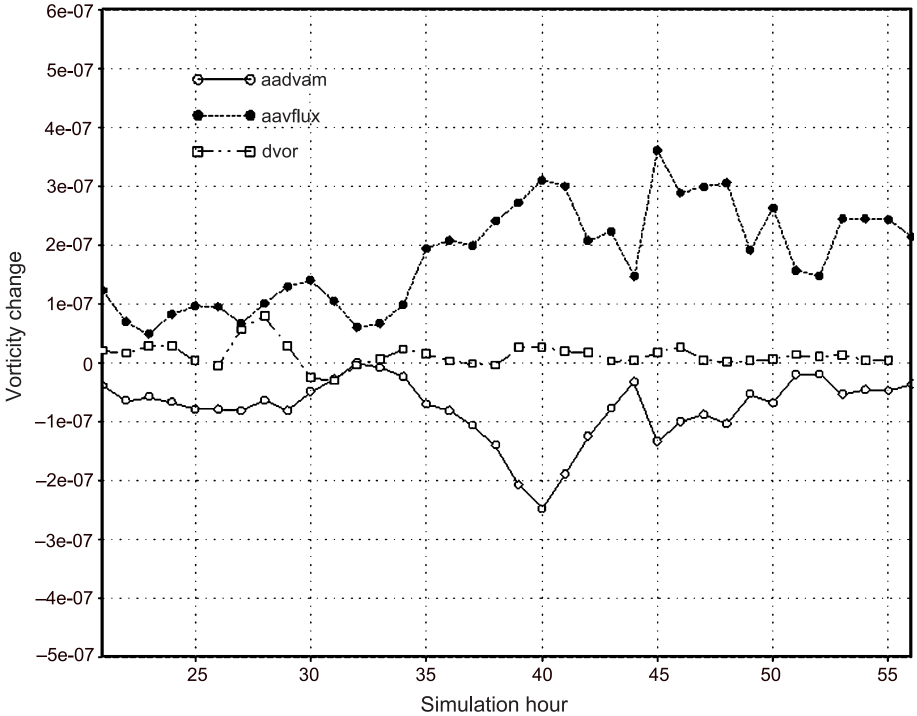

Fig. 12. Area-averaged plots at $\sigma = 0.95$ of aadvam (vorticity advection + vorticity divergence), aavflux (voriticity tilting term + vertical vorticity advection) and dvor (time rate of change of vorticity) for a 6 by 6 grid point box centered on the point of minimum pressure as in previous figures

ing of MCVs near the core of the storm leads to large increases in the vorticity of the storm.

Figure 11 shows the relative contribution of vorticity tendency terms at different levels from $\sigma = 0.99$ to 0.85. At $\sigma = 0.99$, 0.95, v_{div} is the largest source of vorticity during the 3 RI periods. This indicates that the vortex mergers cause a convergence of vorticity into the core of the storm. Figure 11 also shows that v_{adv} acts to reduce the vorticity and largely counteracts v_{div}. This is because the convergent flow is acting up the mean TC vorticity gradient so that lower vorticity is advected into the core of the storm. The terms involving the vertical velocity (vw_{adv} and v_{tilt}) are relatively small near the surface ($\sigma = 0.99$) because the vertical velocity vanishes there, but become more important as height increases. The tilting term has a similar magnitude to v_{div}. at levels $\sigma = 0.90$ and 0.85. At $\sigma = 0.85$ (Fig. 11d) vw_{adv} acts to increase the vorticity during non-RI periods after RI1. Since this level is above the level of maximum vorticity, the positive vertical vorticity is acting down the vertical gradient in vorticity and hence vorticity is advected upwards into the higher levels. Note that this upward vorticity transport is essential for the continuous development of the storm. At this level v_{div}. is in general largely negative, as the divergent flow is more prevalent (Fig. 8a).

A horizontal vorticity flux term may be introduced by combining v_{div}. and v_{adv}. terms together.

$$v_{\text{flux}} = -\frac{\partial}{\partial x}(u\zeta) - \frac{\partial}{\partial y}(v\zeta). \quad (2)$$

This flux form represents the "true" vorticity merging process, and its temporal evolution well reflects the three RI phases (Fig. 12). Similarly, the sum of the terms vw_{adv} and v_{tilt} leads to a new term named d_{vam}:

$$d_{\text{vam}} = \frac{\partial}{\partial y}\left(w\frac{\partial u}{\partial z}\right) - \frac{\partial}{\partial x}\left(w\frac{\partial v}{\partial z}\right). \quad (3)$$

As seen from Fig. 12, the major vorticity generation term is due to the horizontal vorticity merging, whereas the vertical term is a vorticity sink, primarily transporting the low-level cyclonic vorticity upward, leading to a deepening cyclonic system.

6. Conclusions and discussion

This numerical experiment demonstrated that the model is able to simulate a near-equatorial typhoon with NCEP coarse-resolution atmospheric conditions as its initial input. The model started three days prior to actual TC genesis reported by JTWC, with no initial bogus vortex. The simulated TC reached typhoon strength (as judged by the surface wind field) at 1.7° N, close to the observed genesis latitude, even though it formed 12 hours earlier and moved farther to the north than the actual TC. The physical parameterizations used are similar to those in Braun and Tao (2000).

The formation of this near-equatorial typhoon involves the scale interaction between the large-scale background flow and meso-scale vortices. On the large scale, strong low-level northerly winds associated with cold surges in the western SCS were forced to turn cyclonically near the equator due to the influence of the topographic barriers of the islands of Borneo and Sumatra, and the Malaysian peninsula. The resistance to low-level flows by these geographic features aids in the buildup of cyclonically moving air in the SCS. This cold surge-topography interaction is unique in the SCS, and it is unlikely that a near-equatorial TC could occur anywhere else (Chang et al, 2003).

On the mesoscale, the formation of MCVs within the large-scale cyclonic circulation is crucial. The strong low-level vorticity associated with these MCVs developed rapidly along a clearly defined convergent shear line on the eastern edge of the northerly surge. High PV is generated by convergence and stretching at low levels, further magnified by the gradient in diabatic heating within the convective towers. The advection of the MCVs by the cyclonic convergent background flow built up the PV within the core of the storm genesis region. The merging of the MCVs led to rapid pressure drops and vorticity growth.

Three rapid intensification periods occurred during the TC genesis stage. They occurred when MCVs wrapped into the storm core. These periods are associated with strong low-level convergence and large upward vertical velocities. These periods are also associated with elevated cloud water contents in lower and middle troposphere and high stratiform anvil precipitation rates in the upper troposphere. The high cloud water contents contributed to high latent heating rates that maintained a strong vertical potential temperature gradient below the maximum heating level. The increase in the vertical temperature gradient, combined with increases in vorticity, helped to build up the PV at low levels, with a maximum near $\sigma = 0.9$. The increase in vorticity at low levels was primarily attributed to the horizontal vorticity flux (the sum of the horizontal vorticity divergence and the horizontal vorticity advection). Above the maximum vorticity level, vertical vorticity advection and the tilting/twisting term became of comparable importance, contributing the vertical transport of the vorticity.

The "hot tower" hypothesis (e.g., Montgomery and Enagonio, 1998) provides a valuable framework for describing the formation of this modeled TC. Here we have referred to a general term, MCV, to describe mesoscale and vortical convective circulations (including hot towers) that develop during the genesis period. Consistent with Hendricks et al (2004), MCVs can be viewed as mesoscale areas of high PV in the lower troposphere below diabatic heating maximums. The increase in the PV is closely related to the increase of the vertical gradient in potential temperature below convective heating maximums in areas of intense convection. The numerical experiment showed that the high PV associated with MCVs could persist for several hours after the deep convection ceases.

Three periods of rapid intensification (RI1, RI2, and RI3) were identified during the intensification period. The RI periods occurred when a concentrated PV area wrapped around the circulation and merged into the core of the storm. It appears that because the storm is moving towards the northwest, a MCV is more readily absorbed by the core when it is located to the northwest side of the storm center. The low-level increases in vorticity during the RI periods are due to large horizontal fluxes of vorticity into the storm core. There are evidences of the merging of high PV associated with MCVs into the storm core. The merging process has a significant effect on the track of the storm, acting mainly to slow it down temporarily. The RI periods are often followed by a short period (1–3 hours) of no intensification or weakening.

At upper levels below the widespread upper level stratiform rain, there is a large vertical potential temperature gradient. Periods of the widespread stratiform rain coincided with periods of increase in the vertical gradient in potential temperature at the level where the precipitation evaporates. This illustrates the connection between the stratiform rain and increases in the static stability and thus PV below described in Bister and Emanuel (1997). This stratiform rain mechanism could provide additional triggering process for the development of the vertical "hot towers", the axisymmetrization, and the deepening of cyclonic vorticity.

The maximum vorticity generation occurs between levels $\sigma = 0.95$ and 0.90. A vorticity budget analysis provides insight into how the storm core vorticity is built up. The convergence of vorticity is the largest contributor to vorticity increases in the boundary layer. The outward advection of vorticity tends to oppose the vorticity divergence term. Vigorous convection and enhanced vertical velocities occur during the vortex mergers. This helps enhance convergence within the core of the storm. The tilting term and the vertical advection of vorticity become important above the level of maximum vorticity, which primarily contributed to the upward vorticity transport.

Compared to the other terms, the term involving the planetary vorticity is small during the intensification period. This implies that the planetary vorticity was unimportant in the generation of the near-equatorial TC. The planetary vorticity is known to be important in determining the storm intensification rate and the size of the storm. When the Coriolis force is smaller, air in the boundary layer can penetrate closer to the storm center (DeMaria and Pickle, 1988). This leads to the concentration of diabatic heating near the center of the storm. Our model simulation shows that a convectively driven vortex may be developed at near equatorial latitudes for a short period. The fact that both the observed and modeled storm reached only category one intensity suggests that a near-equatorial vortex is unable to reach a strong intensity.

Without the aid of navy ships and TRMM image, typhoon Vamei (2001) would have not been detected. This suggests that we may have missed some cyclogenesis events in the past. Modeling studies similar to this may be capable of determining where, and under what conditions, these fascinating storms could form.

Acknowledgments

This work was supported by ONR grants N000140310739 and N000140612345. The International Pacific Research Center is partially sponsored by the Japan Agency for Marine-Earth Science and Technology (JAMSTEC). Thanks go to Diane Henderson for her helping to check the manuscript. This is SOEST contribution number [redacted] and IPRC contribution number [redacted].

References

Anthes RA (1982) Tropical cyclones: Their evolution, structure and effects. Meteor Monogr, No. 41, Amer Meteor Soc, 208 pp

Bister M, Emanuel K (1997) The genesis of hurricane Guillermo: TEXMEX analyses and a modeling study. Mon Wea Rev 125: 2662–2682

Braun SA, Tao W-K (2000) Sensitivity of high-resolution simulations of hurricane Bob (1991) to planetary boundary layer parameterizations. Mon Wea Rev 128: 3941–3961

Burk SD, Thompson WT (1989) A vertically nested regional numerical weather prediction model with second-order closure physics. Mon Wea Rev 117: 2305–2324

Chang C-P, Liu CH, Kuo HC (2003) Typhoon Vamei: An equatorial tropical cyclone formation. Geophys Res Lett 30(3): 1150 1-4 (DOI: 10.1029/2002GL016365)

Charney J, Eliassen A (1964) On the growth of the hurricane depression. J Atmos Sci 21: 68–75

DeMaria M, Pickle JD (1988) A simplified system of equations for simulations of tropical cyclones. J Atmos Sci 45: 1542–1554

Dudhia J (1989) Numerical study of convection observed during the winter monsoon experiment using a mesoscale two-dimensional model. J Atmos Sci 46: 3077–3107

Dudhia J (1993) A nonhydrostatic version of the Penn State-NCAR mesoscale model: validation tests and simulation of an Atlantic cyclone and cold front. Mon Wea Rev 121: 1493–1513

Hendricks EA, Montgomery MT, Davis CA (2004) The role of "vortical" hot towers in the formation of tropical cyclone Diana (1984). J Atmos Sci 61: 1209–1232

Holliday CR, Thompson AH (1986) An unusual near-equatorial typhoon. Mon Wea Rev 114: 2674–2677

Holton JR (1992) An introduction to dynamic meteorology. Academic Press, 511 pp

Joint Typhoon Warning Center (2002, 2001) Annual tropical cyclone report, joint typhoon warning center, pearl harbor, HI (available at http://www.npmoc.navy.mil.jtwc/atcr/atcr_archive.html)

Landsea CW (2006) Subject: What is a tropical disturbance, a tropical depression, or a tropical storm?, National Hurricane Center website: http://www.aoml.noaa.gov/hrd/tcfaq/A5.html

Montgomery MT, Enagonio J (1998) Tropical cyclogenesis via convectively forced vortex Rossby waves in a three-dimensional quasigeostrophic model. J Atmos Sci 55: 3176–3207

Padgett G (2001) Gary Padgett's monthly global tropical cyclone summary. http://www.typhoon2000.ph/garyp_mgtcs/dec01.txt

Rotunno R, Emanuel K (1987) An air-sea interaction theory for tropical cyclones. Part II: Evolutionary study using a non-hydrostatic axisymmetric numerical model. J Atmos Sci 44: 542–561

Corresponding authors' address: Tim Li (E-mail: timli@hawaii.edu) Christopher Chambers (E-mail: crc@hawaii.edu), IPRC, Department of Meteorology, University of Hawaii, 2525 Correa Rd., Honolulu, HI 96822, USA

Dear Author,

The goal of our new, more rapid publication procedures is to publish your paper online as quickly as possible. The assigning of a DOI (digital object identifier) at this stage means that the work is fully citeable much earlier than has previously been the case. Please note that final pagination will be added only when articles have been assigned to a printed issue. With respect to the quality of figures in the electronic version, please note that the printed version will be of the usual high quality. For a list of all papers published online so far, please refer to the following web-site (your paper will be added to this list after final correction):

http://link.springer.de/link/service/journals/00703/tocs.htm

Offprint Order

Journal: Meteorology and Atmospheric Physics MS No.:0/824 First Author: C. R. S. Chambers

We will supply the corresponding author with one free copy of the relevant issue.
The order of offprints against payment must be sent in when returning the corrected proofs.
The prices quoted are valid only for authors ordering offprints for their private use.
Please write clearly in capital letters!

NEW **When you order offprints against payment, you are entitled to receive in addition a pdf file of your article for your own personal use.** As this pdf file is sent to you by e-mail, please insert the e-mail address here:

____

I hereby order against payment

☐ **50** ☐ **100** ☐ **200** ☐ **300** ☐ **400** **offprints**

Offprints should be sent to: ______________________________
(Name of person or institution)
____
(Address)
____

Payment will be made by: ______________________________
(Name of person or institution)
____
(Address)
____

(Purchase Order No.) ______________________ (Date/Signature of author) ______________________

☐ Please bill me **(please do not pay for offprints before receipt of invoice!)**

☐ Please charge my credit card ☐ Eurocard / Mastercard ☐ American Express
☐ Visa ☐ Diners Club

No.: ______________________ Valid until: ____ / ____

Signature: ______________________

(In all separate correspondence concerning this order please quote the Journal's title, MS No., and First Author.)

Price list for offprints* Prices include carriage charges (surface mail). Prices are subject to change without notice.

***Customers in foreign EU countries:** Please state your V.A.T. registration number if applicable. Otherwise we have to add 10% V.A.T. to the list prices.

V.A.T. registration number: ______________________

Pages (Figs. incl./excl.)	50 Copies	100 Copies	200 Copies	300 Copies	400 Copies
	EUR	EUR	EUR	EUR	EUR
☐ 1–8	296,–	348,–	482,–	598,–	722,–
☐ 9–16	384,–	436,–	626,–	806,–	998,–
☐ 17–24	462,–	512,–	742,–	972,–	1198,–
☐ 25–32	512,–	564,–	844,–	1098,–	1408,–

Please return your order form to:
SpringerWienNewYork, Production Department, **Sachsenplatz 4-6, P.O. Box 89, 1201 Wien, Austria**

Copyright Transfer Statement

The copyright to this article is hereby transferred to Springer (for US Government employees: to the extent transferable), effective if and when the article is accepted for publication. The copyright transfer covers the exclusive rights to reproduce and distribute the article, including reprints, photographic reproductions, microform, electronic database, videodiscs, or any other reproductions of similar nature, and translations.
However, the authors reserve:

1. All proprietary rights other than copyrights, such as patent rights.
2. The right to use all or part of this article in future works of their own and to grant or refuse permission to third parties to republish all or part of the article or translations thereof. To republish whole articles, such third parties must obtain written permission from Springer as well. However, Springer may grant rights concerning journal issues as a whole.

To be signed by at least one of the authors who agrees to inform the others, if any.

____
(Author's signature)

Instruction to printer	Mark	Examples: In the text	Examples: In the margin
Character to be corrected	/	Latter to be corrected	e /
Group of characters to be corrected	H	Letters to be correcting	ed H
Several identical characters to be corrected	/	Cauncil ar Cammission	o ///
Differentiation of several errors in the same paragraph	/ ⌐ F L ⅃	There are many faults in thas lane	r / m⌐ i L a F i ⅃
Character or word to be deleted		Commissiion and and Parliament	
Character or word to be added	⋏	A word missing	is ⋏
Superior character required	^	The Court's judgment.	(1) /
Omitted text to be added (see copy)	⋏	1. January 12. December	⋏ Out see copy
Inferior character required	v	H_2SO	4 /
Change to italic	___	Ad infinitum	ital
Change italic characters to roman	⬭	*status quo*	rom
Change capitals to lower case	⬭	UNESCO	l.c.
Change to capitals or small capitals	≡ =	Robert burns, AD 1759-96	Caps. s.c.
Change to bold face	~~~~	This word needs emphasising!	bold
To be letter-spaced		This needs space	/
Correct horizontal alignment		This line is crooked	/
Text to be raised or lowered		This is line uneven	/ /
Text to be aligned (to the left)		This text is to be aligned	/
Text to be aligned (to the right)		This text is to be aligned	/
Text to be centred	[ ]	This text is to be centred	[ ] /
Take back to previous line	]	This hyph- en is unnecessary	] /
Text to run on (no new paragraph)		... line. No new paragraph here	/
Take forward to next line	[	This hyp- hen is badly placed	[/
Create new paragraph		... line. A new paragraph should begin here	/
Close up		A sp ace is wrong here	/
Equalise space	/	This spacing is very uneven	/
Add space between words		A spaceis missing here	# /
Reduce space between words		These spaces are too big!	/
Add space between lines	—< #	These lines are too close together —< #	—< #
Reduce space between lines	—>	These lines are too far apart.	—> /
Stet (let original text stand)	.....	This text was corrected in error	✓
Transpose characters		These letters are transpoesd	/
Transpose words		These are words transposed	/
Transpose lines		transposed These lines are	/

NB: A correction made in the text must always have a corresponding mark in the margin, otherwise it may be overlooked when the corrections are made. The same marks should be used, where appropriate, by copy-editors marking up copy. Where instructional words are used in marginal marks, e.g. 'ital.', 'bold', etc., they must always be encircled to show that they are not to be printed.

Bernhard Hofmann-Wellenhof, Klaus Legat, Manfred Wieser

Navigation

Principles of Positioning and Guidance

With a contribution by H. Lichtenegger.
2003. XXIX, 427 pages. 99 figures.
Softcover **EUR 54,–.** ISBN 3-211-00828-4

Global navigation satellite systems like GPS or the future European Galileo are influencing the world of navigation tremendously. Today, everybody is concerned with navigation even if unaware of this fact. Therefore, the interest in navigation is increasing.
This book provides an encyclopedic view of navigation. Fundamental elements are presented for a better understanding of the techniques, methods, and systems used in positioning and guidance.
The book is divided into three parts. Besides a historical review and maps, the first part covers mathematical and physical fundamentals. The second part treats the methods of positioning including terrestrial, celestial, satellite-based, inertial, image-based, and integrated navigation. Routing and guidance are the main topics of the third part. Applications on land, at sea, and in the air are considered. The book is designed for students, teachers, and people interested in entering the complex world of navigation.

Bernhard Hofmann-Wellenhof, Herbert Lichtenegger, James Collins

Global Positioning System

Theory and Practice

Fifth, revised edition.
2001. XXIII, 382 pages. 45 figures.
Softcover **EUR 51,–.** ISBN 3-211-83534-2

"... this book [is] an excellent standard reference on GPS for theoreticians and practicians in the future."

Acta Geodaetica, Geophysica et Montanistica Hungarica

Gernot Beer (ed.)

Numerical Simulation in Tunnelling

2003. XVI, 477 pages. Numerous figures, partly in colour.
Hardcover **EUR 110,–.** ISBN 3-211-00515-3

The planned construction of traffic routes through the European Alps represents a challenge for science and technology.
During the past decades, Austria has gained a leading position in the field of tunnelling. This has been verified by many successful projects all over the world, which have been realized with the well-known "New Austrian Tunnelling Method". However, further development and economic success of modern tunnelling methods, which are still partly based on empirical assumptions, can only be assured if their scientific basis is improved. The book discusses the application of numerical simulation methods to assist tunnel engineers. Numerical simulation tools for the estimation of the required tunnel support and the required construction measures are described in this book. By using them, it is possible to study the impact on construction and environment during the planning stage and during construction. This will result in an improvement of the safety and economy of tunnels.

Yong-Qi Chen, Yuk-Cheung Lee (eds.)

Geographical Data Acquisition

2001. XIV, 265 pages. 167 figures.
Softcover **EUR 62,–.** ISBN 3-211-83472-9

This book is dedicated to the theory and methodology of geographical data acquisition, providing comprehensive coverage ranging from the definition of geo-referencing systems, transformation between these systems to the acquisition of geographical data using different methods. Emphasis is placed on conceptual aspects, and the book is written in a semi-technical style to enhance its readability. After reading this book, readers should have a rather good understanding of the nature of spatial data, the accuracy of spatial data, and the theory behind various data acquisition methodologies.

33,3% cheaper for you . . .

As an author of Springer Wien New York you are now entitled to receive a 33,3% price reduction on the list price of all books published by the Springer group. For your order please use this order form. Orders have to be sent directly to Springer Wien New York.

Als Autor/in von Springer Wien New York erhalten Sie 33,3% Rabatt auf den Ladenpreis der **gesamten Buchproduktion** der Springer-Gruppe. Bitte bestellen Sie mit diesem Bestellschien. Ihre Bestellung senden Sie bitte ausschließlich an Springer Wien New York.

For detailed informations about titles published by Springer Wien New York please search our homepage.
Nähere Informationen über das Programm von Springer Wien New York finden Sie auf unserer Homepage.
www.springer.at

Order Form/Bestellschein

Springer Wien New York, Order Department, Sachsenplatz 4–6, P. O. Box 89, 1201 Wien, Austria, Fax +43-1-330 24 26
Springer Wien New York, Auslieferung, Sachsenplatz 4–6, Postfach 89, 1201 Wien, Österreich, Fax +43-1-330 24 26

I order herewith/Ich bestelle hiermit:

copy/ies	ISBN	Author	Title
Expl.	ISBN	Autor	Titel

Please copy this order form for your next orders. Bitte kopieren Sie diesen Bestellschein fur Ihre weiteren Bestellungen.

○ Please bill me/Bitte liefern Sie gegen Rechnung

○ Please charge my credit card/Bitte belasten Sie meine Kreditkarte

○ VISA ○ MASTERCARD ○ AMEX ○ DINERS

Card No./Karten-Nr. ____________________ Expiry date/Gültig bis__________

NAME/NAME ____________________

ADDRESS/ADRESSE ____________________

____

DATE/DATUM ____________________

SIGNATURE/UNTERSCHRIFT ____________________